Journal of Geophysical Research: Planets

RESEARCH ARTICLE
10.1002/2018JE005539

The Penetration of Solar Radiation Into Carbon Dioxide Ice

H. E. Chinnery[1], A. Hagermann[1,2], E. Kaufmann[1,2], and S. R. Lewis[1]

[1]Department of Physical Sciences, The Open University, Milton Keynes, UK, [2]Now at Department of Biological and Environmental Sciences, University of Stirling, Stirling, UK

Key Points:
- The *e*-folding scale for pure CO_2 slab ice has been measured using simulated solar irradiation (wavelengths 300 to 1,100 nm) for the first time
- We suggest the use of 47.6 mm for the average *e*-folding scale of CO_2 ice when modeling the thermophysics of Mars' polar caps
- Applications include the modeling of cryoventing as a formation mechanism for spiders and ephemeral furrows in the Martian polar regions

Supporting Information:
- Supporting Information S1

Correspondence to:
H. E. Chinnery,
hannah.chinnery@open.ac.uk

Citation:
Chinnery, H. E., Hagermann, A., Kaufmann, E., & Lewis, S. R. (2018). The penetration of solar radiation into carbon dioxide ice. *Journal of Geophysical Research: Planets*, *123*, 864–871. https://doi.org/10.1002/2018JE005539

Received 23 JAN 2018
Accepted 13 MAR 2018
Accepted article online 25 MAR 2018
Published online 6 APR 2018

Abstract Icy surfaces behave differently to rocky or regolith-covered surfaces in response to irradiation. A key factor is the ability of visible light to penetrate partially into the subsurface. This results in the solid-state greenhouse effect, as ices can be transparent or translucent to visible and shorter wavelengths, while opaque in the infrared. This can lead to significant differences in shallow subsurface temperature profiles when compared to rocky surfaces. Of particular significance for modeling the solid-state greenhouse effect is the *e*-folding scale, otherwise known as the absorption scale length, or penetration depth, of the ice. While there have been measurements for water ice and snow, pure and with mixtures, to date, there have been no such measurements published for carbon dioxide ice. After an extensive series of measurements we are able to constrain the *e*-folding scale of CO_2 ice for the cumulative wavelength range 300 to 1,100 nm, which is a vital parameter in heat transfer models for the Martian surface, enabling us to better understand surface-atmosphere interactions at Mars' polar caps.

Plain Language Summary The solid-state greenhouse effect is similar to the climatic greenhouse effect. It occurs in solid materials that are translucent, such as ices. On Mars, there is both water ice and carbon dioxide ice. These ices exist on the surface and in the subsurface (similar to permafrost found on Earth). This means light can penetrate through the surface of the ice and transport energy into the ice. The subsurface gets warmer as a result. The extent of the warming effect can be determined by measuring the penetration depth of the sunlight, otherwise known as the *e*-folding scale. In this study we have measured the *e*-folding scale of slabs of carbon dioxide ice, in order to determine how much light can penetrate to a reference depth in the ice. This will allow for more accurate calculations to be made about surface processes that occur on Mars, which have no equivalents on Earth.

1. Introduction

Carbon dioxide ice is a major component of the seasonal ice caps on Mars. Each autumn and winter, around one-third of the atmosphere condenses out to form the polar cap. In the southern polar regions, extensive CO_2 slab ice gives rise to the formation of dark spots and fans, known as dendritic troughs, or "spiders," during ice cap retreat (Kieffer, 2007; Pilorget et al., 2011, 2013; Portyankina et al., 2012). Similar features, described as seasonal furrows, formed by CO_2 jets have been observed in the northern polar region (Bourke, 2013; Bourke & Cranford, 2011; Portyankina, Hansen, & Aye, 2017), although these are erased each year due to sand transportation by summer winds, unlike in the south, where they tend to reoccur in the same locations year on year. Additionally, a wide-spread diurnal CO_2 frost cycle has been discovered (Piqueux et al., 2016), and CO_2 frost and ice has been linked to a number of surface processes, such as gully formation (Diniega et al., 2013; Dundas et al., 2017; Pilorget & Forget, 2015), which is an ongoing process today.

A solid-state greenhouse effect (SSGE) was first described by Matson and Brown (1989), who discussed the importance of broad-spectrum solar radiation propagating into icy surfaces to depths significant in comparison to the diurnal skin depth for thermal diffusion. Based on the hypothesis of Kieffer (2000) that a large-grained slab of CO_2 ice covers the Cryptic region during the southern winter and spring, Piqueux, Bryne, and Richardson (2003) were the first to define and map the distribution of the "spider" features observed in the southern polar region, confirming the correlation of spiders with the existence of highly transparent CO_2 slab ice, which overlies the poorly consolidated particulate regolith of the south polar layered deposits. Kieffer et al. (2006) expanded on this, reporting that the spots and fans observed in the southern polar regions of Mars are associated with surface temperatures consistent with that of CO_2 ice (~145 K) based on Mars Odyssey Thermal Emission Imaging System data, combined with anomalously low albedos. These conditions persist for at least 120 sols following sunrise after the polar winter. Based on this, they proposed a formation mechanism for spot and channels (which form radially around the spots). The seasonal ice cap

forms an impermeable and translucent slab, which undergoes basal sublimation due to extended solar irradiation during the spring. This trapped CO_2 gas eventually overcomes the cryostatic pressure, rupturing the overlying ice and causing high-velocity vents which carry particulate material along with the gas to the surface. This erodes the radial channels in the regolith and transports material to the surface to form the depositional fans. These features are observed in the same locations year on year. This process has since been explored and expanded upon further by studies, such as Kieffer (2007), Pilorget et al. (2011), Martínez et al. (2012), and Pilorget et al. (2013). Additionally, Kaufmann and Hagermann (2017) conducted a series of experiments which reproduced dust eruptions from a dust layer within a slab of CO_2 ice, by irradiating samples under Martian conditions. However, in order to model this phenomenon, the extent of the SSGE in translucent CO_2 slab ice needs to be quantified.

While there have been some experiments done to determine the optical, mechanical, and thermal properties of solid CO_2, many of those are nonideal. Most have used micrometer to millimeter-sized samples (e.g., Hudgins et al., 1993; Quirico & Schmitt, 1997; etc.), which is insufficient to give bulk parameters suitable for large scale models, others suffered from impure samples (Egan & Spagnolo, 1969), or from highly cracked samples (Ditteon & Kieffer, 1979). In addition, many studies focused on determining the optical properties within discrete wavelength ranges (e.g., Hansen, 1997). While CO_2 ice absorbs in narrow bands in the infrared similar to that of CO_2 gas (Hansen, 1999) and has a strong absorption continuum in the ultraviolet, absorption in the visible range is low (Warren, 1986).

Some similar measurements have been made using water ice. Studies using naturally occurring Antarctic sea ice include those made by Brandt and Warren (1996), Perovich (1996), and Datt et al. (2015), focusing on the implications for thermal profiles and subsurface heating on Earth. Others have more of a focus on icy bodies in space, ranging from comets to icy moons to the polar regions of Mars, including Kömle et al. (1990) and Kaufmann, Kömle, and Kargl (2006). However, these also focused on water ice, either pure or with admixtures, and most of these report on the depth of temperature maxima, rather than specifying the *e*-folding scale (with the exception of Kaufmann, Kömle, and Kargl (2006), who suggest an *e*-folding scale of 15 mm for water ice fits their model). Further measurements have been made for the *e*-folding scale of water snow. However, the light transmission regime is heavily influenced by scattering in snow, and so is not considered a useful comparison here. Here we present our findings for the *e*-folding scale, or penetration depth of CO_2 slab ice, which could be applicable for use in models such as those developed by Kieffer (2007) or Pilorget et al. (2011). Kieffer models the formation of CO_2 jets in the Martian polar cap, which leads to the creation of dendritic "spiders." The thermal model by Pilorget et al. (2011), which builds on and develops this concept further, ultimately shows that a formation mechanism involving basal sublimation of the ice sheet which leads to ice rupture and jetting of material onto the surface is plausible based on known parameters. By updating any of these parameters, of which the penetration depth (*e*-folding scale) of solar irradiation in CO_2 slab ice is important, future models can be improved.

2. Theory

The subsurface thermal profile of a body is dependent on the physical and thermal properties of the surface material, and incoming energy fluxes, both external (solar radiation) and internal (geothermal gradient). If the surface material is icy, then the SSGE is an important factor in determining this subsurface thermal profile. The extent of the SSGE is determined by multiple factors, including the optical properties of the icy material, grain size and shape, impurities, depth of ice, etc. However, the penetration depth of solar radiation into the ice is dependent on the absorption scale length or *e*-folding scale (ζ). This also happens to be one of the most poorly understood parameters governing heat transfer in ices (Möhlmann, 2010).

Brandt and Warren (1993) show that radiation is only attenuated exponentially in a purely absorbing medium with no internal scattering. However, if a uniform material which both scatters and attenuates has a sufficient optical depth, the absorption is approximately exponential (Kaufmann & Hagermann, 2015). For water snow, scattering by snow grains (and possibly contaminants) can dramatically reduce light penetration, but the *e*-folding scale will be significantly greater in compact ice. Kaufmann, Kömle, and Kargl (2006) give a value of 1.5 cm for the *e*-folding scale of water slab ice, although they point out a possible range of values up to 10 cm and point out that the *e*-folding scale of CO_2 ice is likely to be even larger. This large range of values can be explained by the variability of ice translucence of samples in this size range. Therefore, measurements

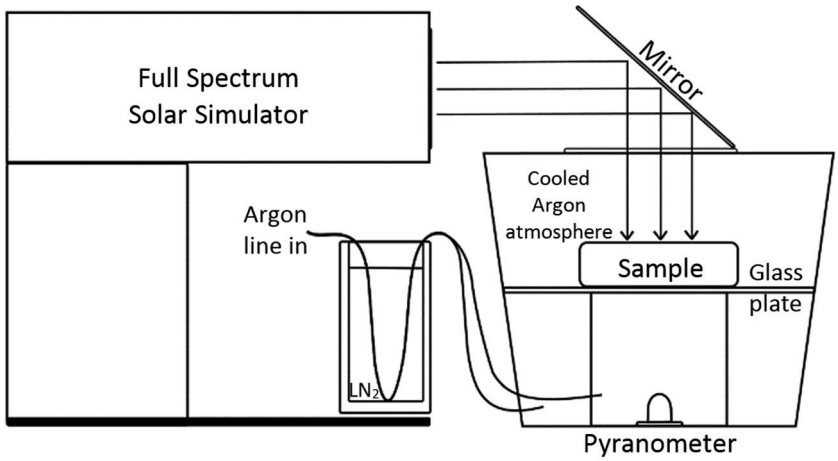

Figure 1. Schematic of experimental setup for CO_2 ice *e*-folding scale measurements.

need to take place over a range of thicknesses to ensure sufficient coverage of the exponential attenuation regime. The downward directed energy flux (F), as a function of ice thickness (x) and the *e*-folding scale (ζ), is defined as

$$F(x) = e^{-x/\zeta} \tag{1}$$

If the intensity of the light propagating through the material decreases rapidly, whether due to scattering or absorption, this will result in a small *e*-folding scale, and vice versa.

The lack of comprehensive *e*-folding scale measurements, especially for materials other than water ice, makes modeling the energy balance and heat transfer for icy planetary surfaces such as that found on Mars very difficult. In addition to this, there are large variations in reported *e*-folding scales due to the effects of impurities, inhomogeneities, and particle shapes and sizes, all of which can be difficult to control within a sample. These effects can lead to models predicting greater transmission in the visible and near-ultraviolet (Beaglehole et al., 1998), or an underestimate of energy absorbed at shallow depths while overestimating absorption at greater depths (Libois et al., 2014). This highlights the need for further measurements in this field, with a special focus on CO_2 ice for improvements to models for heat transfer and surface processes applicable to Mars.

3. Measurements

CO_2 ice samples were prepared by condensing CO_2 directly from the gas phase within a pressure vessel cooled by liquid nitrogen, following the methodology detailed in Kaufmann and Hagermann (2017). This forms large CO_2 ice blocks, which were then cut to size and polished smooth prior to experiment commencement. This polishing minimizes surface scattering of light due to an uneven interface between air and ice. Resizing and polishing of the ice was repeated for each thickness measured. The average densities of the prepared samples were ~1,500 kg m^{-3}.

Experiments were undertaken in an argon-filled chamber, which was first cooled with liquid nitrogen. This both reduced the sublimation rate of the CO_2 ice and minimized water frost deposition on both the sample and the glass plate the sample is placed on.

The sample was irradiated using a full spectrum solar simulator (LS1000R3, Solar Light Company), with the beam directed via a mirror to penetrate the sample perpendicular to the polished surface of sample (see Figure 1). This lamp simulates the spectrum of solar radiation without the influence of the Earth's atmosphere, and so is a good approximation to the irradiation received on Mars but does not account for the effects of Mars' atmospheric composition, clouds, or suspended dust. Based on the work by Singh and Flanner (2016), the albedo of CO_2 snow is much higher in the near-infrared than that of water snow, and so it is logical to suggest that clouds composed of CO_2 would reflect a greater proportion of the near-IR than would occur under H_2O clouds. The transmitted irradiation was then measured using a pyranometer (CS300, Campbell

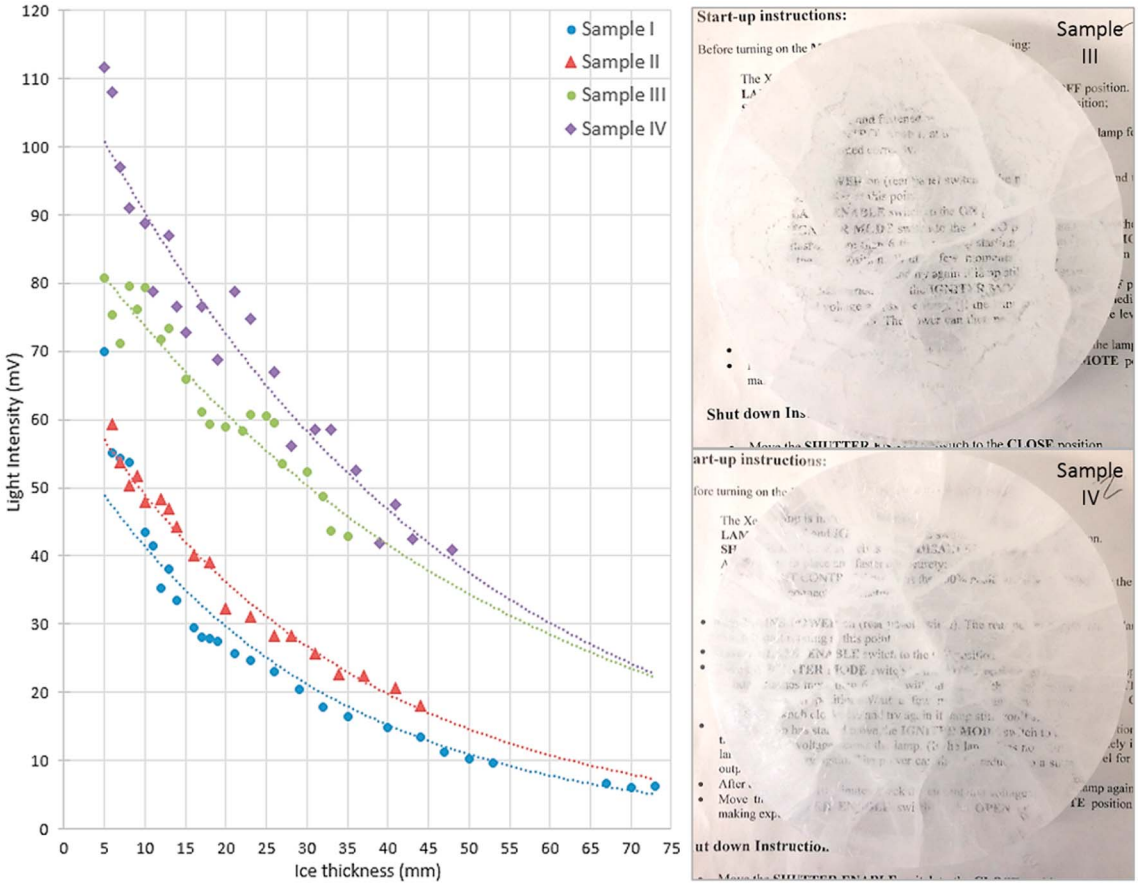

Figure 2. (left) Mean light intensity data plotted against ice thickness, with exponential curves plotted in dotted lines. These are an approximate fit to demonstrate these data can be modeled by an exponential function. (top right) Sample 3 at a thickness of 26 mm, overlying text to demonstrate transparency. This is a standard method of visually judging transparency of ice samples, first reported by Behn (1900). (bottom right) Sample 4 at a thickness of 26 mm, overlying the same example text.

Scientific Ltd.) able to detect wavelengths from 300 to 1,100 nm. It is important to note that *e*-folding scale measurements are independent of total irradiance, although this was found to be quite consistent when measured with the pyranometer prior to the experiment commencement for each sample, varying from 119.7 to 123.5 mV.

Four measurements were made at each ice thickness: one in the center of the sample and three further measurements at different points, approximately 120° offset from center. This ensured that the measurements were made over a range of cracked and clear ice, which should therefore be representative of the ice conditions which occur naturally. This is consistent with the findings of Hansen (1999), who reported how some areas of the seasonal CO_2 caps evolve with time (and increasing insolation through early spring) from low albedo and high emissivity to brighter, fractured, and lower emissivity regions.

Reliable albedo measurements are difficult to obtain, and so, to avoid these additional uncertainties, only measurements made using a minimum thickness of ice are considered in the calculations. This is consistent with the methods of Kaufmann and Hagermann (2015).

4. Results and Discussion

The four measurements made at different locations in the sample for each sample ice thickness have been averaged and plotted in Figure 2. We estimate errors in ice thickness to be ±1 mm, with errors in light intensity readings to be negligible in comparison. While there is some scatter, the data can be approximated to the exponential curve fitted to each sample data set.

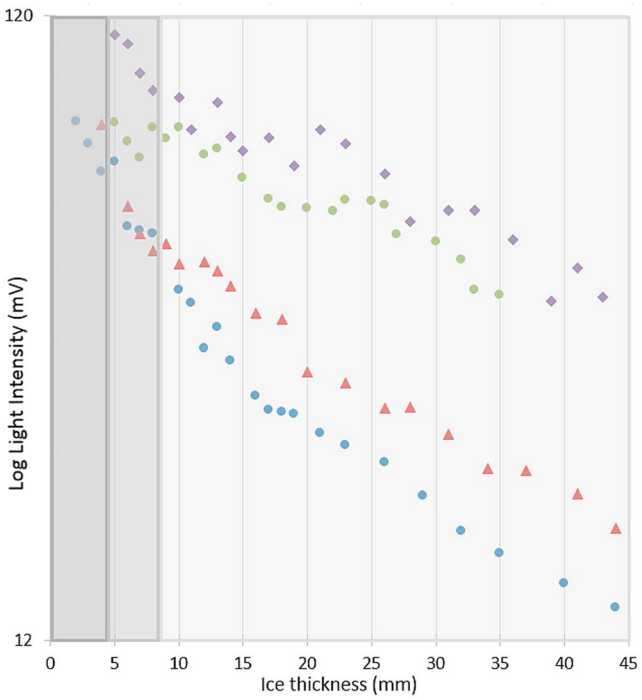

Figure 3. The average light intensity measurements plotted for each sample thickness, including all data points (darkest shading), implementing a 5 mm thickness cutoff (midshading), as used for the *e*-folding scale measurements of water snow by Kaufmann and Hagermann (2015), and a 8-mm cutoff (rest of data). The data should approximate to a straight line when plotted against the log of light intensity, and it can be seen the measurements made using the thinnest of samples deviate from this linear trend consistently. The point at which this deviation begins was identified as 8 mm.

As each sample was prepared and used, the technique was refined and better quality, more transparent ice was produced. This accounts for the general increase in intensity of light propagating through the samples. Figure 2 shows samples 3 and 4 at the same thickness. It is important to note that, while sample 4 appears to have a greater amount of cracks through it, in between the cracks, the ice is more transparent than in sample 3, which has a more clouded or milky appearance, especially outward of the center. This is reflected in the data, with overall better light propagation through the sample and significantly higher light intensities at smaller ice thicknesses.

In order to calculate the *e*-folding scale from light intensity measurements, Kaufmann and Hagermann (2015) used 5 mm of snow thickness for their measurements. However, as ice is more transparent than snow, a greater thickness will be required for these *e*-folding scale measurements. After studying the data, an example using the average data points for each sample thickness can be seen in Figure 3. It was decided 8 mm should be sufficient to reliably eliminate albedo variations. The inclusion of the light intensity measurements from samples $<$8 mm thick can alter the *e*-folding scale results from 3% to 20%, based on our results. Subsequently, 8 mm is taken as the zero point $x = 0$, with all other measurements normalized accordingly. Further to this, all tests were made within a black chamber, which shielded from ambient radiation and minimized reflections which could interfere with the results.

However, on closer inspection of these data, it can be seen that there are some sudden drops in light intensity at certain thicknesses through individual samples. This trend is even more pronounced when studying the raw data—especially the minimum and maximum values. Consequently, these have been plotted in Figure 4. By analyzing the data in this way, we can identify when the large cracking events occurred in the samples (example of the effect of cracking on light intensity measurements shown red). Cracks due to thermal expansion were a problem throughout the duration of these experiments and seem to be a common problem reported in the literature when making measurements with CO_2 ice (e.g., Portyankina et al., 2016). This is because CO_2 ice has a large thermal expansion coefficient (Manzhelii et al., 1971), which is an order of magnitude greater than that of water ice. This results in cracking which temporarily negates the increase in transparency with decreasing ice thickness, and so complicates the data analysis. The more transparent and better quality the sample at the start, the more cracking episodes occur, and the greater the effect on the light penetration measurements. This is why samples 3 and 4 allow for better light penetration overall, but the data are more scattered.

As a consequence, we have conducted the *e*-folding scale calculations on an exponential curve fitted to the data, repeated for the minimum light intensity measurements—representative of highly cracked ice or "milky" ice states; maximum light intensity measurements—representative of the most ideal and transparent samples, and then the average light intensity measurements. This range of different states for the ice samples have value, as they are representative of the different states of a natural ice slab as it would occur in the Martian polar regions. Here the ice caps are thought to evolve over time from low albedo smooth slab ice through to bright, highly fractured ice in the Martian spring (Hansen, 1999).

The *e*-folding scale calculated using minimum light intensity measurements for samples 1 and 2 is higher than that calculated using the maximum data (see Table 1). This can be explained by the fact that these samples started out more opaque or "milky," and so light penetration was lower than in the other samples. As measurements commenced, the minimum amount of light able to penetrate through the sample increased steadily. However, additional cracks would reduce the maximum light intensity, and so the rate of increase in light penetration was slower than that for the minimum results. In contrast, samples 3 and 4 were much more

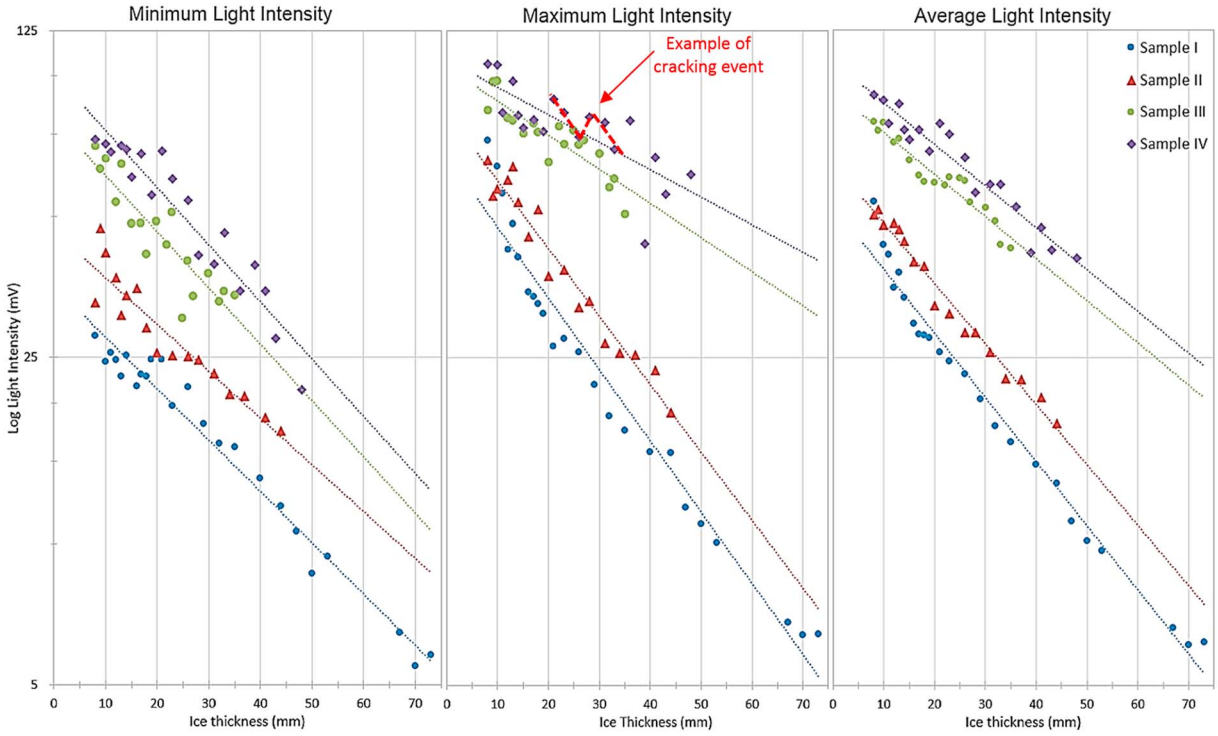

Figure 4. The (left) minimum, (middle) maximum, and (right) mean measurements of light intensity through CO_2 ice samples are plotted at varying ice thicknesses. A line of best fit is plotted, and the exponential function of this line is then used to calculate the *e*-folding scale. Much of the scatter around these lines are due to cracking events within the ice sample (e.g., if all 4 measurements happen to have been made over cracks rather than perfect ice, the maximum light intensity which is possible to pass through the sample will not have been recorded).

transparent at the beginning, and so any cracks forming would affect the minimum and maximum readings more equally than in samples 1 and 2. Consequently, we have more confidence in the results obtained from samples 3 and 4.

We therefore find that it is reasonable to give an *e*-folding scale value of $\zeta = 35.7 \pm 7.7$ mm for cracked, higher albedo CO_2 ice. For perfectly smooth, unblemished slab ice $\zeta = 65.1 \pm 6.3$ mm would be more applicable. However, we would urge caution with using the highest estimations of the *e*-folding scale, for in reality, any thermal variations, such as the diurnal insolation cycle, are likely to cause thermal cracking of the CO_2 slab ice. One possible application of this would be at the end of the polar night in the "Cryptic" region, with a thick, clean CO_2 ice slab, as described by Pilorget et al. (2011), which is rapidly followed by the onset of dark spot, or spider, formation, which then contaminates the ice with dust from the underlying regolith. For other scenarios where the slab would be illuminated diurnally with solar radiation, we would recommend the use of $\zeta = 47.6$ mm for an average CO_2 ice slab.

Table 1
e-Folding Scale Results Based on the Minimum, Maximum, and Mean Light Intensity Measurements for Each Sample

	e-Folding scale, ζ (mm)		
Sample no.	Min intensity	Max intensity	Mean intensity
1	40.00	28.57	32.58
2	43.48	30.30	33.33
3	35.71	58.82	47.62
4	35.71	71.43	47.62

5. Conclusions

The *e*-folding scale of pure CO_2 slab ice has been investigated using broad spectrum solar radiation. While *e*-folding scale values range from 35.7 ± 7.7 mm to 65.1 ± 6.3 mm, we would recommend the use of 47.6 mm for "normal" conditions. This is due to the large amount of thermal cracking which occurs during irradiation of the ice. This means that the upper value range is applicable for fresh, stable slab ice which exhibits minimal cracking, such as that seen in the polar regions in early to midwinter on Mars. Equally, the lower values for the *e*-folding scale are appropriate for settings where highly cracked and thermally altered CO_2 slab ice occurs, as observed in late winter time and early spring during ice cap retreat, when dendritic troughs (spiders) and dark spots appear due to the increase in diurnal temperatures, which results in a much greater amount of thermal cracking and higher albedo conditions (Hansen, 1999).

Acknowledgments
This work was funded by STFC under grant no. ST/N50421X/1, with additional support from grant no. ST/L000776/1. Access to the full data set generated in these experiments can be found in the supporting documentation. The authors thank the two reviewers for their very helpful comments which helped greatly improve this manuscript.

References

Beaglehole, D., Ramanathan, B., & Rumberg, J. (1998). The UV to IR transmittance of Antarctic snow. *Journal of Geophysical Research*, *103*, 8849–8857. https://doi.org/10.1029/97JD03604

Behn, U. (1900). Ueber die Dichte der Kohlensäure im festen und flüssigem Zustande. *Annalen der Physik*, *308*(12), 733–743. https://doi.org/10.1002/andp.19003081209

Bourke, M., & Cranford, A. (2011). Seasonal formation of furrows on polar dunes, Fifth Mars Polar Science Conference: 6059.

Bourke, M. C. (2013). The formation of sand furrows by cryo-venting on Martian dunes, 44th Lunar and Planetary Science Conference: 2919.

Brandt, R. E., & Warren, S. G. (1993). Solar-heating rates and temperature profiles in Antarctic snow and ice. *Journal of Glaciology*, *39*(131), 99–110. https://doi.org/10.1017/S0022143000015756

Datt, P., Gusain, H. S., & Das, R. K. (2015). Measurements of net subsurface heat flux in snow and ice media in Dronning Maud Land, Antarctica. *Journal Geological Society of India*, *86*(5), 613–619. https://doi.org/10.1007/s12594-015-0352-y

Diniega, S., Hansen, C. J., McElwaine, J. N., Hugenholtz, C. H., Dundas, C. M., McEwen, A. S., & Bourke, M. C. (2013). A new dry hypothesis for the formation of Martian linear gullies. *Icarus*, *225*(1), 526–537. https://doi.org/10.1016/j.icarus.2013.04.006

Ditteon, R., & Kieffer, H. (1979). Optical properties of solid CO_2: Application to Mars. *Journal of Geophysical Research*, *84*, 8294–8300. https://doi.org/10.1029/JB084iB14p08294

Dundas, C. M., McEwen, A. S., Diniega, S., Hansen, C. J., Byrne, S., & McElwaine, J. N. (2017). The formation of gullies on Mars today. *Geological Society of London, Special Publications*, SP467.5. https://doi.org/10.1144/SP467.5

Egan, W. G., & Spagnolo, F. A. (1969). Complex index of refraction of bulk solid carbon dioxide. *Applied Optics*, *8*(11), 2359–2360. https://doi.org/10.1364/AO.8.002359

Hansen, G. B. (1997). The infrared absorption spectrum of carbon dioxide ice from 1.8 to 333 μm. *Journal of Geophysical Research*, *102*, 21,569–21,587. https://doi.org/10.1029/97JE01875

Hansen, G. B. (1999). Control of the radiative behavior of the Martian polar caps by surface CO_2 ice: Evidence from Mars Global Surveyor measurements. *Journal of Geophysical Research*, *104*, 16,471–16,486. https://doi.org/10.1029/1998JE000626

Hudgins, D. M., Sandford, S. A., Allamandola, L. J., & Tielens, A. G. G. M. (1993). Mid- and far-infrared spectroscopy of ices—Optical constants and integrated absorbances. *Astrophysical Journal Supplement Series*, *86*(2), 713–870. https://doi.org/10.1086/191796

Kaufmann, E., & Hagermann, A. (2015). Penetration of solar radiation into pure and Mars-dust contaminated snow. *Icarus*, *252*, 144–149. https://doi.org/10.1016/j.icarus.2015.01.007

Kaufmann, E., & Hagermann, A. (2017). Experimental investigation of insolation-driven dust ejection from Mars' CO_2 ice caps. *Icarus*, *282*, 118–126. https://doi.org/10.1016/j.icarus.2016.09.039

Kaufmann, E., Kömle, N., & Kargl, G. (2006). Laboratory simulation experiments on the solid-state greenhouse effect in planetary ices. *Icarus*, *185*(1), 274–286. https://doi.org/10.1016/j.icarus.2006.07.009

Kieffer, H. H. (2000). Annual punctuated CO_2 slab-ice and jets on Mars, Mars. *Polar Science*, 4095.

Kieffer, H. H. (2007). Cold jets in the Martian polar caps. *Journal of Geophysical Research*, *112*, E08005. https://doi.org/10.1029/2006JE002816

Kieffer, H. H., Christensen, P. R., & Titus, T. N. (2006). CO_2 jets formed by sublimation beneath translucent slab ice in Mars' seasonal south polar ice cap. *Nature Letters*, *442*(7104), 793–796. https://doi.org/10.1038/nature04945

Kömle, N., Deetleff, G., & Dankert, C. (1990). Thermal behaviour of pure and dusty ices on comets and icy satellites. *Astronomy and Astrophysics*, *277*, 246–254.

Libois, Q., Picard, G., Dumont, M., Arnaud, L., Sergent, C., Pougatch, E., et al. (2014). Experimental determination of the absorption enhancement parameter of snow. *Journal of Glaciology*, *60*(222), 714–724. https://doi.org/10.3189/2014JoG14J015

Manzhelii, V. G., Tolkachev, A. M., Bagatskii, M. I., & Voitovich, E. I. (1971). Thermal expansion, heat capacity, and compressibility of solid CO_2. *Physica Status Solidi*, *44*(1), 39–49. https://doi.org/10.1002/pssb.2220440104

Martínez, G. M., Renno, N. O., & Elliott, H. M. (2012). The evolution of the albedo of dark spots observed on Mars polar region. *Icarus*, *221*(2), 816–830. https://doi.org/10.1016/j.icarus.2012.09.008

Matson, D. L., & Brown, B. H. (1989). Solid-state greenhouses and their implications for icy satellites. *Icarus*, *77*(1), 67–81. https://doi.org/10.1016/0019-1035(89)90007-9

Möhlmann, D. T. F. (2010). Temporary liquid water in upper snow/ice sub-surfaces on Mars? *Icarus*, *207*(1), 140–148. https://doi.org/10.1016/j.icarus.2009.11.013

Perovich, D. K. (1996). *The optical properties of sea ice*, *Monograph 96–1*. Cold Regions Research & Engineering Laboratory. Springfield, VA: Office of Naval Research.

Pilorget, C., Edwards, C. S., Ehlmann, B. L., Forget, F., & Millour, E. (2013). Material ejection by the cold jets and temperature evolution of the south seasonal polar cap of Mars from THEMIS/CRISM observations and implications for surface properties. *Journal of Geophysical Research: Planets*, *118*, 2520–2536. https://doi.org/10.1002/2013JE004513

Pilorget, C., & Forget, F. (2015). Formation of gullies on Mars by debris flows triggered by CO_2 sublimation. *Nature Geoscience*, *9*(1), 65–69.

Pilorget, C., Forget, F., Millour, E., Vincendon, M., & Madeleine, J. B. (2011). Dark spots and cold jets in the polar regions of Mars: New clues from a thermal model of surface CO_2 ice. *Icarus*, *213*(1), 131–149. https://doi.org/10.1016/j.icarus.2011.01.031

Piqueux, S., Bryne, S., & Richardson, M. I. (2003). Sublimation of Mars's southern seasonal CO_2 ice cap and the formation of spiders. *Journal of Geophysical Research*, *108*(E8), 5084. https://doi.org/10.1029/2002JE002007

Piqueux, S., Kleinböhl, A., Hayne, P. O., Heavens, N. G., Kass, D. M., McCleese, D. J., et al. (2016). Discovery of a widespread low-latitude diurnal CO_2 frost cycle on Mars. *Journal of Geophysical Research: Planets*, *121*, 1174–1189. https://doi.org/10.1002/2016JE005034

Portyankina, G., Hansen, C. J., & Aye, K.-M. (2017). Present-day erosion of Martian polar terrain by the seasonal CO_2 jets. *Icarus*, *282*, 93–103. https://doi.org/10.1016/j.icarus.2016.09.007

Portyankina, G., Merrison, J., Iversen, J., Yoldi, Z., Hansen, C. J., Aye, K.-M., & Pommerol, A. (2016). Laboratory investigations of physical state of CO_2 ice on Mars, Sixth Mars Polar Science Conference.

Portyankina, G., Pommerol, A., Aye, K.-M., Hansen, C. J., & Thomas, N. (2012). Polygonal cracks in the seasonal semi-translucent CO_2 ice layer in Martian polar areas. *Journal of Geophysical Research*, *117*, E02006. https://doi.org/10.1029/2011JE003917

Quirico, E., & Schmitt, B. (1997). Near-infrared spectroscopy of simple hydrocarbons and carbon oxides diluted in solid N_2 and as pure ices: Implications for Triton and Pluto. *Icarus*, *127*(2), 354–378. https://doi.org/10.1006/icar.1996.5663

Singh, D., & Flanner, M. G. (2016). An improved carbon dioxide snow spectral albedo model: Application to Martian conditions. *Journal of Geophysical Research: Planets*, *121*, 2037–2054. https://doi.org/10.1002/2016JE005040

Warren, S. G. (1986). Optical constants of carbon dioxide ice. *Applied Optics*, *25*(16), 2650–2674. https://doi.org/10.1364/AO.25.002650